Oral presentation | Data science and AI

Data science and AI-I

Wed. Jul 17, 2024 4:30 PM - 6:30 PM Room C

[9-C-03] Field Inversion and Symbolic Regression Augmented Spalart-Allmaras Model for Airfoil

*Zizhou He[1], Yufei Zhang[1] (1. School of Aerospace Engineering, Tsinghua University)

Keywords: Airfoil Stall, Discrete Adjoint, Field Inversion, Symbolic Regression

Twelfth International Conference on Computational Fluid Dynamics (ICCFD12), Kobe, Japan, July 14-19, 2024

Field Inversion and Symbolic Regression Augmented Spalart-Allmaras Model for Airfoil Stall Prediction

Zizhou He* and Yufei Zhang*
Corresponding author: zhangyufei@tsinghua.edu.cn
* School of Aerospace Engineering, Tsinghua University, China

Abstract: The accuracy of airfoil stall prediction largely depends on the simulation of separated flows. Numerous data-driven turbulence modeling methods have been proposed to improve the flow separation prediction accuracy of the Reynolds-averaged Navier-Stokes method. However, traditional machine learning models based on neural networks often lack physical interpretability. In this paper, the symbolic regression (SR) method is adopted to establish an analytic expression mapping between local flow field variables and the Spalart-Allmaras (SA) model correction factor β to enhance the SA model's predictive performance under stall conditions. Field inversion based on the discrete adjoint method is used to obtain training data. Moreover, the expression is obtained using symbolic regression. The SA model embedded with the β expression is referred to as the SA-SR model, which can be integrated into computational fluid dynamics solvers with minimal increase in computational load. The generalization capability of the SA-SR model is tested under a variety of different cases, demonstrating its ability to accurately predict attached flows while correcting stall flows within a certain range.

Keywords: Field Inversion, Symbolic Regression, Airfoil Stall, Machine Learning.

1 Introduction

Airfoil stall is a common phenomenon in engineering practice of aerodynamics [1]. It is generally caused by flow separation due to large angle of attack (AOA), which results in a significant decrease in the lift-to-drag ratio of the airfoil [2]. Since stall is primarily related to the separation of the suction surface boundary layer under adverse pressure gradient flow, the key to accurately predicting stall in computational fluid dynamics (CFD) is the precise computation of separation under adverse pressure gradient [3].

Numerous experiments have revealed significant unsteady and three-dimensional effects in trailing-edge stall flows [4,5]. These complexities render existing Reynolds-averaged Navier–Stokes (RANS) method incapable of producing accurate results [6]. Therefore, many unsteady methods such as direct numerical simulation (DNS) and large eddy simulation (LES) have been applied to this problem [7,8]. However, considering computational costs, modifying existing RANS turbulence models to accurately predict stall remains the most economical approach in engineering applications [9]. Following traditional turbulence modeling approaches, modifications can be made to turbulence models to address adverse pressure gradient flows [10]. Nevertheless, this task heavily relies on the modelers' experience.

In recent years, data-driven methods have been widely used to address the poor predictive performance of turbulence models in complex flows [11–13]. A notably representative achievement is the framework proposed by Duraisamy et al. [14], which combined adjoint-based turbulence model uncertainty quantification and machine learning correction, known as the field inversion and machine learning (FIML). However, traditional data-driven methods often utilize black-box models like artificial neural network (ANN), which lack physical interpretability. This limits the exploration of the physical mechanisms for corrections and the manual adjustments. To address these issues, symbolic regression (SR) method has been attempted in the process of data-driven turbulence modeling. Previous studies [15,16] have utilized SR method for turbulence modeling to enhance the models' predictive capacity in certain complex flow scenarios. However, most research has primarily focused on correcting models within separated shear layers, with relatively limited effective application to problem within adverse pressure gradient boundary layers.

In this paper, similar to the FIML framework proposed by Duraisamy, we add a correction factor β to the production term of the Spalart-Allmaras (SA) model transport equation. The discrete adjoint method is used for flow field inversion under several conditions of the S809 airfoil to obtain the β dataset. Subsequently, this dataset is fitted using SR to derive an explicit expression of β as a function of local flow field variables. Finally, the physical mechanisms of this expression are analyzed, and its generalization performance is validated on test cases different from the S809 airfoil. The results demonstrate its promising application prospects for addressing airfoil stall issues under adverse pressure gradient separation.

2 Methodology

In this study, the flow field inversion method is utilized to obtain the distribution of correction factor. Subsequently, the symbolic regression method is employed to fit the expression of the correction factor.

2.1 Field inversion

The equation for the Spalart-Allmaras (SA) model constructed by Spalart is as follows [17]:

$$\frac{\mathrm{D}\tilde{\nu}}{\mathrm{D}t} = P - D + \frac{1}{\sigma}\left[\nabla\cdot((\nu+\tilde{\nu})\nabla\tilde{\nu}) + C_{b2}(\nabla\tilde{\nu})^2\right], \tag{1}$$

where the P and D are the production and destruction terms, respectively. The research by Duraisamy et al. [14] suggested that multiplying a correction factor β in front of the production term P in Eq. (1) can improve the model's prediction of separated flows. Thus, Eq. (1) becomes:

$$\frac{\mathrm{D}\tilde{\nu}}{\mathrm{D}t} = \beta(\boldsymbol{x})\cdot P - D + \frac{1}{\sigma}\left[\nabla\cdot((\nu+\tilde{\nu})\nabla\tilde{\nu}) + C_{b2}(\nabla\tilde{\nu})^2\right]. \tag{2}$$

The distribution of β over the spatial coordinate $\boldsymbol{x}$ can be obtained through the following flow field inversion process:

$$\min_{\beta} J = \sum_i \lambda_{\mathrm{obs},i}(d_i - h_i(\boldsymbol{\beta}))^2 + \sum_j \lambda_{\mathrm{prior},j}(\beta_j - 1)^2. \tag{3}$$

The optimization problem in Eq. (3) involves a large number of variables, necessitating the use of gradient optimization algorithms. Therefore, the discrete adjoint method [18] is applied in this study to reduce computational cost. It decouples the cost of gradient computations from the number of variables. In this study, the open-source solver ADflow [19] with secondary development is used for RANS equations and adjoint equations calculations.

2.2 Symbolic regression

A mapping relationship between the correction factor β and local physical features needs to be established to modify the SA model under different cases. Symbolic regression method is utilized to fit the expression between the following physical features [11,12,16] and the offset of β(i.e., $\beta - 1$):

$$
\begin{aligned}
&x_0 = \frac{\tilde{\nu}}{\nu} = \chi, && x_1 = \log\left(\frac{\tau}{\tau_{ref}} + \varepsilon\right), && x_2 = 1 - \tanh\left(\sqrt{r_d}\right) = f_d', \\
&x_3 = \log\left(\frac{P}{D+\varepsilon} + \varepsilon\right), && x_4 = \log\left(\frac{\left|\nabla\tilde{\nu}\right| d}{\nu + \tilde{\nu}} + \varepsilon\right), && x_5 = \frac{|\mathbf{\Omega}|}{|\mathbf{S}|}, \\
&x_6 = tr\left(\hat{\mathbf{S}}^2\right) = \lambda_1, && x_7 = -tr\left(\hat{\mathbf{\Omega}}^2\right) = -\lambda_2, && x_8 = tr\left(\hat{\mathbf{\Omega}}^2 \cdot \hat{\mathbf{S}}^2\right) = \lambda_3, \\
&x_9 = \left|\hat{\mathbf{\Omega}}\right|, && x_{10} = \frac{|\mathbf{\Omega}| d^2}{\nu} = \mathrm{Re}_\Omega, && x_{11} = \log(|\nabla\hat{p}| + \varepsilon),
\end{aligned} \tag{4}
$$

The symbolic regression library PySR [20] is used to fit the expression from local physical quantities to $\beta - 1$, which employs genetic algorithms to optimize the form of expressions. Finally, PySR provides the optimal results under different complexities. It is up to the user to choose which to adopt based on metrics such as the degree of fit and complexity.

3 Results and Discussion

3.1 Field inversion and symbolic regression

Field inversion is performed on the S809 airfoil under condition of $Ma = 0.1\ and\ Re = 2 \times 10^6$, with the objective of determining the spatial distribution of the correction factor β. Firstly, the performance of the baseline SA model at various AOA (α) is tested, and the results in Fig. 1 demonstrate its ability to accurately predict C_L in the linear range while failing in stall conditions. The experimental results for the C_L are sourced from the Delft University of Technology Low Speed Laboratory [21].

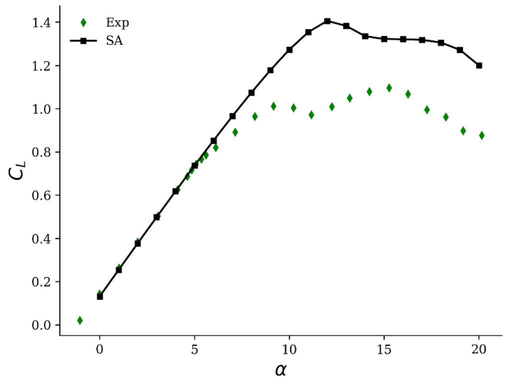

Fig. 1. Prediction of the C_L for the S809 airfoil by the baseline SA model ($Ma = 0.1\ and\ Re = 2 \times 10^6$).

We use the C_L as the QoI and, following the weighting coefficient settings by Yan et al. [13], perform field inversion under conditions of $\alpha = 8.2°\ and\ 14°$. Therefore, the objective function for the inversion process is shown in Eq.(5). To ensure that the corrections are more likely to occur within the adverse pressure gradient boundary layer on the suction surface rather than in the separation bubble, we set λ_{prior} as specified in Eq. (6), where $x = 1.0$ represents the x-coordinate of the airfoil's trailing edge.

$$\min_{\beta} J = (C_{L,\mathrm{Exp}} - C_{L,\mathrm{pridi}}(\boldsymbol{\beta}))^2 + \lambda_{\mathrm{prior}} \sum_j (\beta_j - 1)^2. \tag{5}$$

$$\lambda_{prior} = \begin{cases} 2.5 \times 10^{-5}, x \le 1.0 \\ 2.5 \times 10^{-3}, x > 1.0 \end{cases}. \tag{6}$$

After the iterations of the field inversion, the distributions of the correction factor β in the inversion flow fields are shown in Fig. 2, where it can be seen that the eddy viscosity on the suction surface of the airfoil is reduced. As illustrated in Fig. 3, this results in an earlier separation point of the flow, thereby enlarging the separation bubble and consequently leading to a decrease in the predicted C_L.

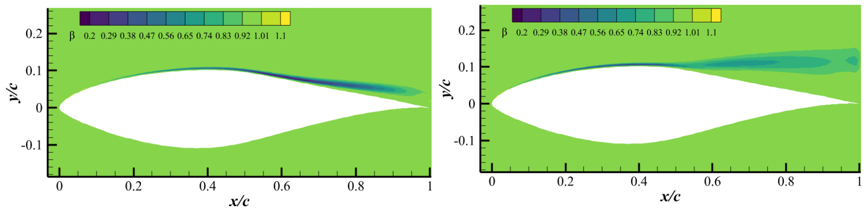

(a) $\alpha = 8.2°$ **(b) $\alpha = 14°$**

Fig. 2. Distribution of β in the inversion results ($Ma = 0.1$ *and* $Re = 2 \times 10^6$).

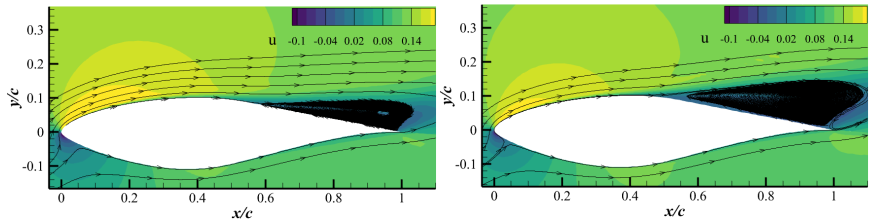

(a) SA **(b) FI**

Fig. 3. Comparisons of flow fields in the inversion results ($Ma = 0.1, Re = 2 \times 10^6, \alpha = 14°$).

Next, explicit expressions will be generated by PySR using the features from Eq. (4) and the operators listed in Table 1. After iterations of the genetic algorithm, expressions of varying complexity were obtained. Balancing complexity and fitting accuracy, we selected Eq. (7) as the result of symbolic regression.

Table 1. The operators used for symbolic regression.

Operator Type	Operators
Unary operators	$\exp(x)$, $\tanh(x)$
Binary operators	$x + y, x - y, x * y, x/y$

$$\begin{aligned} \beta_{SR} &= \beta^*_{SR} + 1 \\ &= 0.00042 * \tanh(x_8) * \frac{x_0^2}{x_6} + 1 \\ &= 0.00042 * \tanh(\lambda_3) * \frac{\chi^2}{\lambda_1} + 1 \end{aligned} \tag{7}$$

An important physical insight is that in the stall flow around the airfoil, the pressure gradient is a critical feature. However, Eq. (7) does not include this feature. To ensure that the correction is only applied in adverse pressure gradient flows, we refer to Wu's study [16] and add a switch function based on the pressure gradient to Eq. (7), modifying it to:

$$\begin{aligned} \beta_{SR} &= \beta^*_{SR} S_p + 1, \\ S_p &= \frac{1}{2} * tanh\left(C_{sp,1} * \left(x_{11} + C_{sp,2}\right)\right) + \frac{1}{2} \\ &= \frac{1}{2} * tanh\left(C_{sp,1} * \left(\log(|\nabla \hat{p}| + \varepsilon) + C_{sp,2}\right)\right) + \frac{1}{2}, \\ C_{sp,1} &= 2, C_{sp,2} = 15. \end{aligned} \tag{8}$$

In Eq. (8), S_p is referred to as the pressure gradient switch function. It determines whether to activate the correction by assessing the value of x_{11} from Eq. (4). The β expression incorporating this switch function, denoted as Eq. (8), is termed the SA-SR model. It will be embedded within the CFD solver to adjust the calculations of the SA model.

3.2 Validation and generalization of the SA-SR model.

In this section, the accuracy of the SA-SR model in predicting stall flow will be tested in the actual CFD solving process. Initially, the SA-SR model is applied to the same conditions as the training data ($Ma = 0.1, Re = 2 \times 10^6, and\ \alpha = 14°$), resulting in the β distribution shown in Fig. 4. It can be observed that the SA-SR model produced a β distribution essentially identical to the inversion result shown in Fig. 2(b).

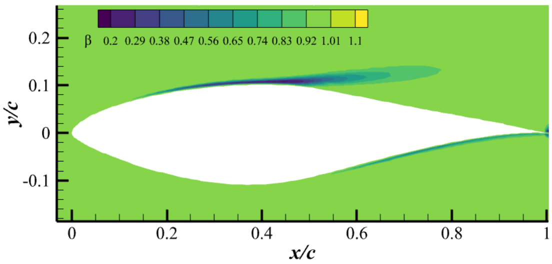

Fig. 4. β distribution for the S809 airfoil predicted by the SA-SR model ($Ma = 0.1, Re = 2 \times 10^6, and\ \alpha = 14°$).

Next, the SA-SR model is used to predict C_L and the drag coefficient (C_D) of the S809 airfoil at $Ma = 0.1\ and\ Re = 2 \times 10^6$ across different AOAs. The results from Fig. 5(a) show that the current model accurately predicted the AOA at which the S809 airfoil begins to stall and the C_L after stall, while maintaining the baseline SA model's accurate prediction for non-stall conditions. From Fig. 5(b), although C_D information was not introduced during the inversion process, the SA-SR model still accurately correct the baseline SA model's prediction of the polar curve's turning point. Therefore, the current results demonstrate that the SA-SR model can maintain the accuracy of the baseline SA model in predicting attached flow while correcting its prediction of separated flow. This reflects the generalization ability of the current SA-SR model at different AOAs.

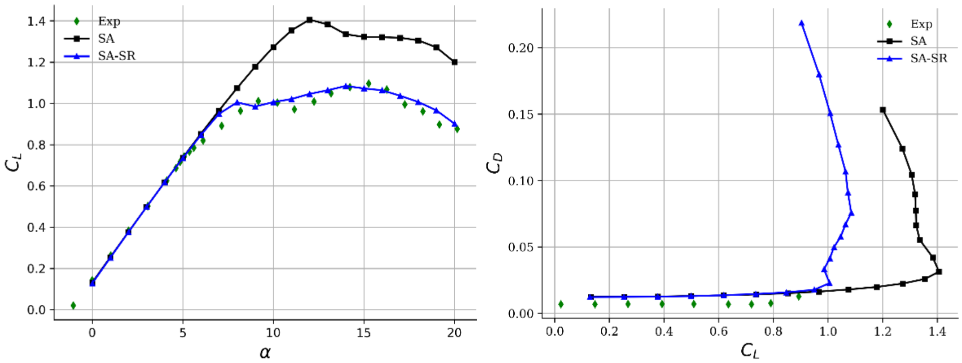

(a) C_L curve. **(b) C_D curve.**

Fig. 5. C_L and C_D curves for the S809 airfoil predicted by the SA-SR model ($Ma = 0.1\ and\ Re = 2 \times 10^6$).

Further tests are conducted on the S805 and S825 airfoils, which have different geometric shapes from the S809 airfoil, with the inflow conditions remaining at $Ma = 0.1\ and\ Re = 2 \times 10^6$. Fig. 6 shows the C_L at different AOAs for these two airfoils, predicted by the SA-SR model, with experimental data sourced from reports by Somers et al. [22,23] It is evident that the SA-SR model, even when applied to airfoils different from those in the training data, still ensures accurate prediction of stall AOAs and C_L.

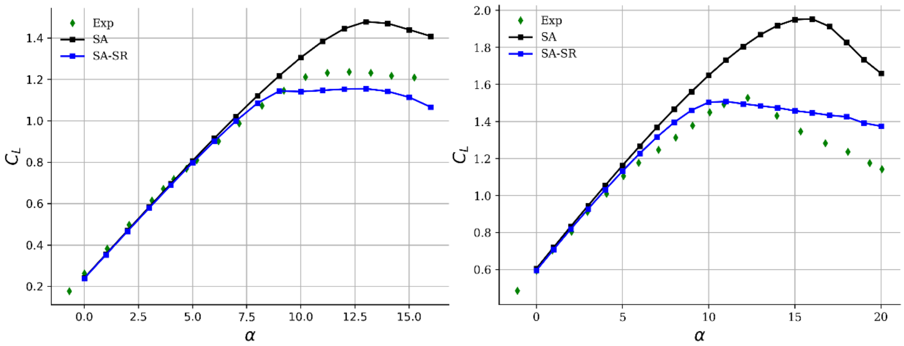

(a) S805 airfoil. **(b) S825 airfoil.**

Fig. 6. C_L curves for the S805 and S825 airfoils predicted by the SA-SR model ($Ma = 0.1$ *and* $Re = 2 \times 10^6$).

Fig. 7 presents a comparison of the flow fields for the S805 and S825 airfoils at $\alpha = 12°$, as predicted by the SA-SR model, against the baseline SA model results. It is evident that the SA-SR model still corrects the C_L by enlarging the separation bubble. Additionally, Fig. 7 clearly shows that although the S805 and S825 airfoils belong to the same series as the S809 airfoil, they have significant differences in their geometric shapes. Therefore, the accurate prediction of the C_L for the S805 and S825 airfoils by the SA-SR model demonstrates its generalization ability across different airfoil geometries.

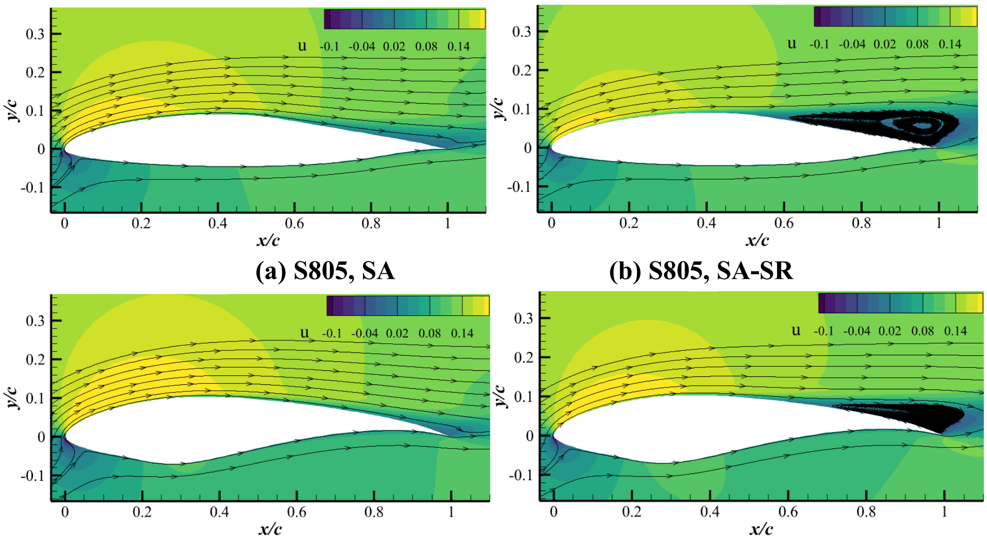

(a) S805, SA **(b) S805, SA-SR**

(c) S825, SA **(d) S825, SA-SR**

Fig. 7. Flow fields for the S805 and S825 airfoils predicted by the SA-SR model ($Ma = 0.1$, $Re = 2 \times 10^6$, *and* $\alpha = 12°$).

However, when we attempted to validate the SA-SR model under a more diverse set of conditions, the results are not entirely satisfactory. On the S809 airfoil case at $Ma = 0.1$ *and* $Re = 1 \times 10^6$, the SA-SR model predicted the C_L curve as shown in Fig. 8. The figure shows that at Re lower than those in the training data, the SA-SR model still predicts stall angles and C_L that are too high. In other words, the SA-SR model does not sufficiently correct the baseline SA model.

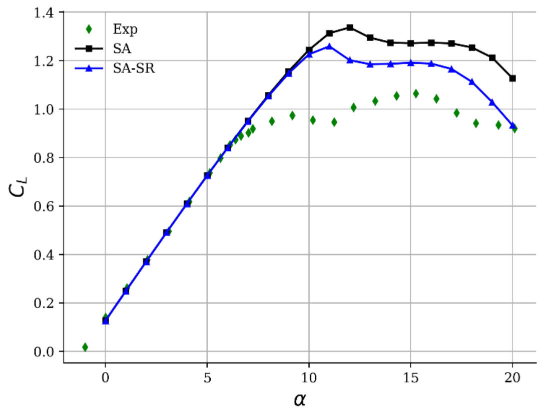

Fig. 8. C_L curve for the S809 airfoil predicted by the SA-SR model ($Ma = 0.1$ *and* $Re = 1 \times 10^6$)

The results from Fig. 8 indicate that the current SA-SR model has limited generalization capability across different conditions. To address this issue, one strategy could be to expand the dataset to include flow fields at different Re. However, in practice, the β distributions obtained from inversions at different Re vary, making it challenging for symbolic regression to effectively and uniformly fit them. Additionally, the efficiency of genetic algorithms tends to decrease as the number of samples increases, which further complicates the fitting process. Therefore, finding a method to effectively enhance the generalization ability of the current SA-SR model under various conditions will be a key issue that we need to address in the future.

4 Conclusions and Future Work

This paper utilizes the field inversion method with the discrete adjoint method and symbolic regression to develop a stall prediction model for airfoils based on the SA model, termed the SA-SR model. The model is integrated into the CFD solver ADflow and has been tested across different AOAs and airfoil geometries, demonstrating its good generalization capability and validating the feasibility of the current framework. However, the model performed poorly in test cases at different Re, indicating its weak generalization capability across various conditions. Our next steps will involve efforts to enhance the generalization ability of the SA-SR model and to further validate it under a broader range of test cases.

References

[1] A. Choudhry, R. Leknys, M. Arjomandi, and R. Kelso, *An Insight into the Dynamic Stall Lift Characteristics*, Experimental Thermal and Fluid Science **58**, 188 (2014).

[2] C. Lindenburg, *Stall Coefficients. Aerodynamic Airfoil Coefficients at Large Angles of Attack*, (2001).

[3] Y. Tamaki, Y. Fukushima, Y. Kuya, and S. Kawai, *Physics and Modeling of Trailing-Edge Stall Phenomena for Wall-Modeled Large-Eddy Simulation*, Phys. Rev. Fluids **5**, 074602 (2020).

[4] W. Geissler and H. Haselmeyer, *Investigation of Dynamic Stall Onset*, Aerospace Science and Technology **10**, 590 (2006).

[5] A. P. Broeren and M. B. Bragg, *Spanwise Variation in the Unsteady Stalling Flowfields of Two-Dimensional Airfoil Models*, AIAA Journal **39**, 1641 (2001).

[6] A. Celic and E. H. Hirschel, *Comparison of Eddy-Viscosity Turbulence Models in Flows with Adverse Pressure Gradient*, AIAA Journal **44**, 2156 (2006).

[7] K. Asada and S. Kawai, *Large-Eddy Simulation of Airfoil Flow near Stall Condition at Reynolds Number 2.1 × 106*, Physics of Fluids **30**, 085103 (2018).

[8] S. M. Hosseini, R. Vinuesa, P. Schlatter, A. Hanifi, and D. S. Henningson, *Direct Numerical Simulation of the Flow around a Wing Section at Moderate Reynolds Number*, International Journal of Heat and Fluid Flow **61**, 117 (2016).

[9] A. A. Matyushenko and A. V. Garbaruk, *Adjustment of the K- ω SST Turbulence Model for Prediction of Airfoil Characteristics near Stall*, J. Phys.: Conf. Ser. **769**, 012082 (2016).

[10] C. Wu, H. Li, Y. Zhang, and H. Chen, *Prediction of Airfoil Stall Based on a Modified K−v2‾−ω Turbulence Model*, Mathematics **10**, 272 (2022).

[11] Y. Yin, Z. Shen, Y. Zhang, H. Chen, and S. Fu, *An Iterative Data-Driven Turbulence Modeling Framework Based on Reynolds Stress Representation*, Theoretical and Applied Mechanics Letters **12**, 100381 (2022).

[12] C. Yan, Y. Zhang, and H. Chen, *Data Augmented Turbulence Modeling for Three-Dimensional Separation Flows*, Physics of Fluids **34**, 075101 (2022).

[13] C. Yan, H. Li, Y. Zhang, and H. Chen, *Data-Driven Turbulence Modeling in Separated Flows Considering Physical Mechanism Analysis*, International Journal of Heat and Fluid Flow **96**, 109004 (2022).

[14] A. P. Singh, S. Medida, and K. Duraisamy, *Machine-Learning-Augmented Predictive Modeling of Turbulent Separated Flows over Airfoils*, AIAA Journal **55**, 2215 (2017).

[15] H. Tang, Y. Wang, T. Wang, and L. Tian, *Discovering Explicit Reynolds-Averaged Turbulence Closures for Turbulent Separated Flows through Deep Learning-Based Symbolic Regression with Non-Linear Corrections*, Physics of Fluids **35**, 025118 (2023).

[16] C. Wu and Y. Zhang, *Enhancing the Shear-Stress-Transport Turbulence Model with Symbolic Regression: A Generalizable and Interpretable Data-Driven Approach*, Phys. Rev. Fluids **8**, 084604 (2023).

[17] P. Spalart and S. Allmaras, *A One-Equation Turbulence Model for Aerodynamic Flows*, in *30th Aerospace Sciences Meeting and Exhibit* (1992), p. 439.

[18] E. J. Nielsen and W. K. Anderson, *Aerodynamic Design Optimization on Unstructured Meshes Using the Navier-Stokes Equations*, AIAA Journal **37**, 1411 (1999).

[19] G. K. Kenway, C. A. Mader, P. He, and J. R. Martins, *Effective Adjoint Approaches for Computational Fluid Dynamics*, Progress in Aerospace Sciences **110**, 100542 (2019).

[20] M. Cranmer, *Interpretable Machine Learning for Science with PySR and SymbolicRegression.Jl*, arXiv:2305.01582.

[21] D. M. Somers, Design and Experimental Results for the S809 Airfoil, National Renewable Energy Lab.(NREL), Golden, CO (United States), 1997.

[22] D. M. Somers, Design and Experimental Results for the S805 Airfoil, 1997.

[23] D. M. Somers, Design and Experimental Results for the S825 Airfoil Period of Performance: 1998–1999 Design and Experimental Results for the S825 Airfoil, Technical Report NREL/SR-500-36346, National Renewable Energy Laboratory …, 2005.